Evidence for a ferryl intermediate in a heme-based dioxygenase

Ariel Lewis-Ballester[a], Dipanwita Batabyal[a], Tsuyoshi Egawa[a], Changyuan Lu[a], Yu Lin[a], Marcelo A. Marti[b,c], Luciana Capece[b], Dario A. Estrin[b], and Syun-Ru Yeh[a,1]

[a]Department of Physiology and Biophysics, Albert Einstein College of Medicine, 1300 Morris Park Avenue, Bronx, NY 10461; and [b]Departamento de Química Inorgánica, Analítica y Química Física/Instituto de Química de los Materiales, Medio Ambiente y Energía-Consejo Nacional de Investigaciones Científicas y Técnicas, and [c]Departamento de Química Biológica, Facultad de Ciencias Exactas y Naturales, Universidad de Buenos Aires, Ciudad Universitaria, Pabellón 2, Buenos Aires, C1428EHA, Argentina

Edited by Harry B. Gray, California Institute of Technology, Pasadena, CA, and approved August 18, 2009 (received for review June 15, 2009)

In contrast to the wide spectrum of cytochrome P450 monooxygenases, there are only 2 heme-based dioxygenases in humans: tryptophan dioxygenase (hTDO) and indoleamine 2,3-dioxygenase (hIDO). hTDO and hIDO catalyze the same oxidative ring cleavage reaction of L-tryptophan to N-formyl kynurenine, the initial and rate-limiting step of the kynurenine pathway. Despite immense interest, the mechanism by which the 2 enzymes execute the dioxygenase reaction remains elusive. Here, we report experimental evidence for a key ferryl intermediate of hIDO that supports a mechanism in which the 2 atoms of dioxygen are inserted into the substrate via a consecutive 2-step reaction. This finding introduces a paradigm shift in our understanding of the heme-based dioxygenase chemistry, which was previously believed to proceed via simultaneous incorporation of both atoms of dioxygen into the substrate. The ferryl intermediate is not observable during the hTDO reaction, highlighting the structural differences between the 2 dioxygenases, as well as the importance of stereoelectronic factors in modulating the reactions.

indoleamine 2,3-dioxygenase | reasonance Raman spectroscopy | tryptophan dioxygenase

Hemeproteins constitute one of the most important classes of biomolecules. They provide a foundation for a variety of cellular regulatory, metabolic, and respiratory processes by transferring electrons (e.g., cytochromes), transporting gas molecules (e.g., globins and nitrophorins), sensing gas molecules (e.g., soluble guanylate cyclase and the neuronal PAS domain protein), or performing oxygen reactions (e.g., oxidases and oxygenases). To implement oxygen reactions, the relatively inert dioxygen first has to be activated. In cytochrome P450 monooxygenases, heme iron-bound dioxygen is believed to be activated by a 2 electron-reduction to peroxide that, via heterolytic O-O bond cleavage, converts to an active ferryl species ($Fe^{4+}=O^{2-}$), with a π-cation radical on the porphyrin ring (i.e., the so-called "compound-I species") (1–3). Compound-I is a strong oxidant that is capable of hydroxylation of alkanes or epoxidation of alkenes. In vitro, the dioxygen reaction of P450 can be bypassed by direct binding of hydrogen peroxide to the ferric heme iron, via the well-known peroxide shunt, leading to the same compound-I intermediate with monooxygenase activity. A similar mechanism is believed to be operative in oxidases (4–7), peroxidases, and catalases (8, 9). In contrast, heme-based dioxygenases, including indoleamine 2,3-dioxygenase (IDO) and trypotophan dioxygenase (TDO), insert 2 oxygen atoms into an organic substrate without consuming any electrons (see ref. 3 and references therein). Despite decades of effort, the mechanism by which dioxygen is activated and inserted into the substrate in the dioxygenase reactions is not known, presenting a major knowledge gap in heme oxygen chemistry. Nonetheless, it is generally believed that the 2 atoms of the dioxygen are simultaneously incorporated into the substrate, setting it apart from monooxygenase reactions (1–3).

IDO and TDO catalyze the same oxidative cleavage of tryptophan (Trp) to N-formyl kynurenine (NFK), the initial and rate-limiting step of the kynurenine pathway, by adding both atoms of dioxygen to the $C_2=C_3$ bond of the indole moiety of Trp (Scheme 1) (3, 10–14). Although they catalyze the same reaction, the 2 dioxygenases engage in distinct functions. Human TDO (hTDO) is a hepatic enzyme: it is inducible by glucocorticoid hormones and is critical for the control of the relative Trp flux in the serotonergic and kynurenic pathways (15, 16). In contrast, human IDO (hIDO) is ubiquitously distributed in all tissues other than liver; it is inducible by IFN-γ (10, 17, 18) and plays important immunoregulatory roles in a variety of pathophysiological conditions (3, 18–20).

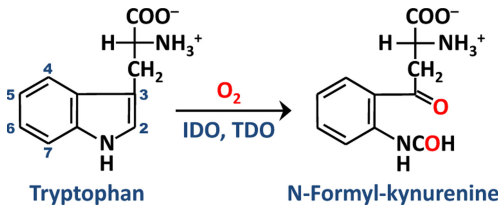

Scheme 1. The dioxygenase reaction catalyzed by IDO and TDO.

Previous studies suggested that the first step of the IDO and TDO reaction involves the deprotonation of the indoleamine group of the substrate by an active site base [Fig. S1] (3, 21, 22), which facilitates the concurrent electrophilic addition of the heme-bound O_2 to the $C_2=C_3$ bond of Trp, thereby leading to the formation of the heme iron-bound 3-indolenylperoxy intermediate. The 3-indolenylperoxy intermediate subsequently converts to the product, NFK, via either a Criegee rearrangement or a dioxetane pathway. A major breakthrough in the understanding of the heme-based dioxygenase chemistry was made recently by the unveiling of the crystallographic structures of hIDO and 2 bacterial isoforms of TDO (23–25). Structure-based sequence alignment shows that the proximal histidine ligand and most of the critical distal residues involved in substrate-protein interactions in TDO are conserved in IDO (24, 25). Spectroscopic studies suggested that the active site base for hTDO is an evolutionarily conserved residue, H76, while that in hIDO is the heme-bound dioxygen (see *SI Text* and Fig. S2) (26–28). Although convincing, the base-catalyzed mechanism has recently been challenged by results derived from density functional theory (DFT) calculations of a heme-Trp model system (29), which

Author contributions: A.L.-B., D.B., T.E., C.L., M.A.M., L.C., D.A.E., and S.-R.Y. designed research; A.L.-B., D.B., T.E., C.L., M.A.M., and L.C. performed research; Y.L. contributed new reagents/analytic tools; A.L.-B., D.B., T.E., C.L., M.A.M., L.C., D.A.E., and S.-R.Y. analyzed data; and A.L.-B., D.B., T.E., C.L., M.A.M., L.C., D.A.E., and S.-R.Y. wrote the paper;.

The authors declare no conflict of interest.

This article is a PNAS Direct Submission.

[1]To whom correspondence should be addressed. E-mail: syun-ru.yeh@einstein.yu.edu.

This article contains supporting information online at www.pnas.org/cgi/content/full/0906655106/DCSupplemental.

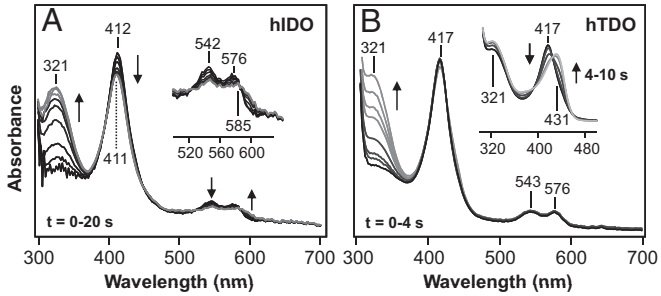

Fig. 1. Time-resolved absorption spectra obtained following the mixing of deoxy hIDO (*A*) or hTDO (*B*) with O_2-containing buffer in the presence of L-Trp in a stopped-flow system. The time-dependent spectra in (*A*) and (*B*) were obtained in the 0 to 20 s and 0 to 4 s time window, respectively. The inset in (*B*) shows the data obtained in the 4 to 10 s time window. The associated kinetic traces are shown in Fig. 2. The inset in (*A*) shows the expanded view of the visible region of the spectra.

show that the basicity of heme-bound O_2 is not strong enough to deprotonate the indoleamine group of the substrate.

In an effort to elucidate the mechanistic details of the dioxygenase reaction, we used continuous-flow resonance Raman (RR) spectroscopy to examine possible oxygen-containing intermediates generated during the dioxygenase reaction of hIDO and hTDO in real time. Our data reveal a ferryl intermediate transiently populated during the reaction of hIDO, demonstrating that the 2 atoms of dioxygen are inserted into the substrate one at a time via a 2-step reaction. Based on these results, combined with classic molecular dynamics and hybrid quantum mechanical and molecular mechanical (QM/MM) simulations, a ferryl-based mechanism is proposed.

Results and Discussion

To determine the appropriate time windows for the continuous-flow RR measurements, we first monitored the hIDO and hTDO reactions, following the mixing of the deoxy enzymes with O_2-containing buffer in the presence of L-Trp, with a stopped-flow system. For hIDO, the reaction was initiated by O_2 binding to the deoxy enzyme to form the active ternary complex, hIDO-O_2-Trp (λ_{max}≈412 nm) (see Fig. 1*A*), which reached completion within ≈80 ms (see *Inset* in Fig. 2*A*). The ternary complex constantly turned over to generate NFK, as indicated by the increase in the intensity of the 321 nm band (30). As the ternary complex is prone to auto-oxidation, via releasing O_2 as superoxide as reported for rabbit IDO (31), NFK formation is concurrent with the gradual production of the ferric enzyme. At the end of the reaction, when all of the O_2 in the solution mixture was consumed, a ferric-like spectrum with λ_{max} at 411 nm was observed.

Likewise, for hTDO, the reaction was initiated by O_2 binding to the deoxy enzyme to form the active ternary complex, hTDO-O_2-Trp (λ_{max} = 417 nm) (see Fig. 1*B*), although, as compared to hIDO, the reaction is significantly faster (which reached completion within the instrument deadtime, ≈1 ms). The ternary complex thus produced constantly turned over to produce NFK (see the 321 nm band) until O_2 was consumed. Unlike hIDO, at the end of the reaction a deoxy enzyme (with λ_{max} = 431 nm) (see *Inset* in Fig. 1*B*), rather than a ferric enzyme, was observed, demonstrating that auto-oxidation is negligible during the hTDO reaction, as illustrated in Fig. 2*C*. The leakage to the ferric species during the multiple turn over of hIDO led to a parabolic, instead of linear, temporal profile of NFK (see Fig. 2 *A* vs. *B*), highlighting the fundamental differences between the 2 dioxygenases.

Oxygen Intermediates of hIDO. On the basis of the stopped-flow data shown in Figs. 1 and 2, we measured the RR spectrum of the ternary complex of hIDO at 200 ms, at the onset of product formation, in real time by using a homemade continuous-flow mixing device (32). As shown in Fig. 3*A*, the RR spectrum of the ternary complex of hIDO is dominated by the strong in-plane and out-of-plane vibrational modes of the heme, as well as the modes associated with the peripheral groups attached to it. The assignments of these modes (33–37) are indicted in Fig. S3. In general, in the RR spectra of heme groups with D_{4h} symmetry, only the totally symmetric A_{1g} in-plane modes are resonance enhanced with Soret excitation (38). The development of various asymmetric in-plane and out-of-plane modes in the ternary complex of hIDO, but not in the substrate-free enzyme (spectra *i* and *ii* in Fig. S3), indicates that substrate-binding causes reduction of the in-plane symmetry and introduces out-of-plane distortion of the porphyrin macrocycle of the heme (39). On the other hand, the enhancement of a vinyl vibrational mode (δ_{vinyl}) at 421 cm^{-1} (see Fig. 3) indicates that the changes in the heme conformation are associated with the movement of the vinyl groups with respect to the porphyrin plane.

To identify the oxygen-associated modes, the same measurements were carried out with $^{18}O_2$. In the $^{16}O_2$–$^{18}O_2$ difference spectra, all of the heme modes are cancelled out; the remaining positive and negative peaks are associated with the ^{16}O- and ^{18}O-related modes, respectively (see spectrum *i* in Fig. 3*A*). Accordingly, the positive peaks at 563 and 1,137 cm^{-1} are assigned to the $\nu_{Fe\text{-}O2}$ and $\nu_{O\text{-}O}$ modes, respectively, similar to those reported for other heme proteins with histidine as a proximal ligand (see ref. 40 and references therein). It is noteworthy that the negative components associated with the 563 cm^{-1} peak exhibit 2 minima at 522 and 538 cm^{-1} because of the coupling of the $\nu_{Fe\text{-}O2}$ mode to an intrinsic heme mode at 526 cm^{-1}, similar to that reported for the oxy-derivative of a globin model system (41). Likewise, the 1,137 cm^{-1} peak appears to be much sharper as compared to its negative component at 1,062 cm^{-1}, possibly because of coupling with transaxial ligand modes (41).

The $\nu_{O\text{-}O}$ mode of heme-bound dioxygen in histidine-coordinated hemeproteins is in general not Raman active. However, it was recently found to be significantly enhanced in several newly discovered truncated hemoglobins (40), a result of the presence of a dynamic H-bonding network between both atoms of the heme-bound O_2 and its surrounding environment; in addition, the enhancement of the $\nu_{O\text{-}O}$ mode was typically found to be associated with a relatively low $\nu_{Fe\text{-}O2}$ frequency at ≈550 to 560

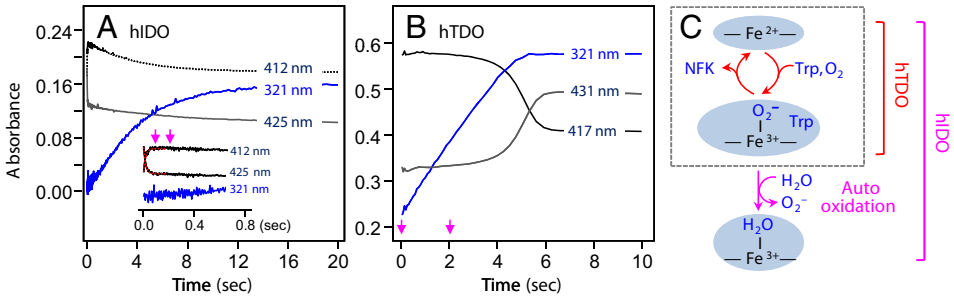

Fig. 2. Kinetic traces (*A* and *B*) associated with the dioxygenase reactions shown in Fig. 1 and a schematic illustration (*C*) of the hIDO and hTDO reactions. The kinetic traces were obtained at the absorption maxima of NFK, the ternary complex and the deoxy enzyme (321, 412, and 425 nm, respectively, for hIDO, and 321, 417, and 431 nm, respectively, for hTDO). The inset in (*A*) is an expanded view of the kinetic traces in the early time window. The traces are offset for clarity. The magenta arrows indicated the time points for the resonance Raman measurements (see text).

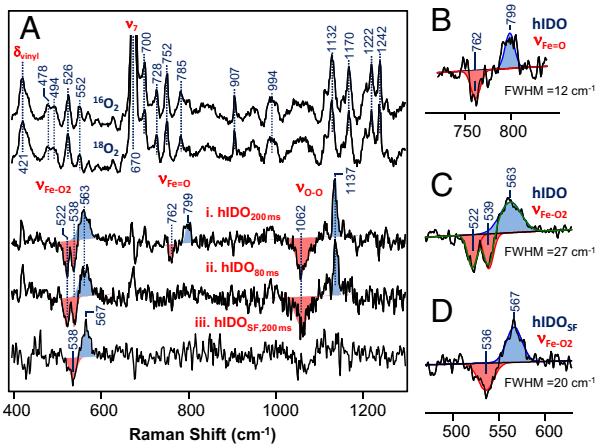

Fig. 3. Resonance Raman spectra obtained following the mixing of deoxy hIDO with O_2-saturated buffer in the presence of L-Trp. The top 2 spectra in (*A*) are the raw data obtained in the presence of $^{16}O_2$ and $^{18}O_2$ at 200 ms. The intensities are normalized with respect to the ν_7 mode. The $^{16}O_2$-$^{18}O_2$ isotope difference spectra (*i* and *ii*) were obtained at 200 and 80 ms; the spectrum (*iii*) was obtained from a substrate-free sample (labeled as "SF") at 200 ms, as a control. The intensities of the isotope difference spectra were normalized based on the $\nu_{Fe\text{-}O2}$ mode. (*B–D*) The expanded view of the $\nu_{Fe\text{-}O2}$ and modes, along with the best-fitted Gaussian curves (*solid lines*). FWHM, full-width at half-maximum. The excitation wavelength was 413.1 nm (32 mW) and the spectral acquisition time was ≈5 min.

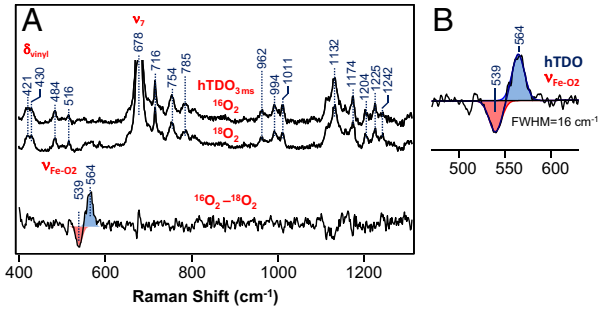

Fig. 4. Resonance Raman spectra obtained following the mixing of deoxy hTDO with O_2-saturated buffer in the presence of L-Trp. The top 2 spectra in (*A*) are the raw data obtained in the presence of $^{16}O_2$ and $^{18}O_2$ at 3 ms. The intensities are normalized with respect to the ν_7 mode. (*B*) The expanded view of the $\nu_{Fe\text{-}O2}$ mode, along with the best-fitted Gaussian curves (*solid lines*). FWHM, full-width at half-maximum. The excitation wavelength was 413.1 nm (5 mW), and the spectral acquisition time was ≈2 min.

cm^{-1}, with respect to the $\nu_{Fe\text{-}O2}$ of mammalian globins at ≈570 cm^{-1} (see ref. 40 and references therein). As such, the unusual activation of the $\nu_{O\text{-}O}$ mode in hIDO, along with its relatively low $\nu_{Fe\text{-}O2}$ frequency, suggests that the heme-bound O_2 accepts multiple H-bonds donated from the substrate or protein matrix surrounding it. Moreover, the frequency of the $\nu_{O\text{-}O}$ mode at 1,137 cm^{-1} demonstrates that the heme-bound O_2 exhibits superoxide character (42), instead of a neutral dioxygen, as was proposed on the basis of the base-catalyzed mechanism (3).

The most remarkable finding revealed by the data shown in Fig. 3*A* is the presence of the 799 cm^{-1} band, characteristic for the $Fe^{4+}{=}O^{2-}$ stretching mode ($\nu_{Fe=O}$) of a compound-II type of ferryl derivative of heme proteins, with histidine as a proximal ligand (see ref. 43 and references therein). Although the $\nu_{Fe=O}$ mode of compound-I type of ferryl species with a porphyrin π-cation radical also lies in this spectral region (44), it was excluded for 2 reasons: (*i*) the characteristic broad Soret band at ≈400 nm and visible band at ≈650 nm for compound-I type of ferryl species (45) were not observed in the transient spectra shown in Fig. 1*A*; and (*ii*) our computational studies indicate a homolytic O-O bond scission following the insertion of the terminal atom of the dioxygen into L-Trp (*vide infra*). It is noteworthy that the $\nu_{O\text{-}O}$ mode of the peroxo derivative of heme proteins with thiolate as a proximal ligand (such as P450 and chloroperoxidase) also appears in the 800 cm^{-1} spectral window (46, 47); the 799 cm^{-1} band is not assigned to a peroxo species because, for histidine-coordinated heme proteins, the $\nu_{Fe\text{-}O}$ mode of the peroxo species should be detectable at ≈617 cm^{-1} (48), while the $\nu_{O\text{-}O}$ mode is typically Raman silent [albeit the $\nu_{O\text{-}O}$ mode of the peroxo derivatives of cobalt-substituted myoglobin has been identified at ≈851 cm^{-1} (49)]. It is important to note that the compound-II type of ferryl derivatives in general exhibit electronic transition bands similar to that of superoxo-ferric complexes (see ref. 43 and references therein), accounting for the fact that no intermediate other than the ternary complex was apparent in the transient spectra shown in Fig. 1*A*.

Additional studies carried out at an earlier time point, 80 ms, show that only the $\nu_{Fe\text{-}O2}/\nu_{O\text{-}O}$ modes at 563/1,137 cm^{-1} of the ferric superoxo intermediate were observable (see spectrum *ii* in Fig. 3*A*), suggesting that the ferryl intermediate is the successor of the superoxo species. Taken together the data indicate that the dioxygenase reaction of hIDO follows a consecutive 2-step mechanism, in which the first atom of the dioxygen molecule is added to the substrate during the superoxo→ferryl transition, while the second oxygen atom is subsequently inserted from the ferryl species into the partially oxidized substrate, yielding the product, NFK. In the absence of the substrate, the ferryl intermediate was not observed (see spectrum *iii* in Fig. 3*A*), and only one $\nu_{Fe\text{-}O2}$ mode at 567 cm^{-1} was identified. The width of the $\nu_{Fe\text{-}O2}$ mode is ≈7 cm^{-1} narrower than that of the ternary complex (see Fig. 3 *C* versus *D*), highlighting the multiconformation nature of the ternary complex (*vide infra*). The 4 cm^{-1} lower $\nu_{Fe\text{-}O2}$ frequency and the absence of the $\nu_{O\text{-}O}$ mode indicate that the presence of substrate perturbs the H-bonding network linked to the heme-bound superoxide.

Oxygen Intermediates of hTDO. On the basis of the stopped-flow data discussed above, we examined the RR spectrum of the ternary complex of hTDO at 3 ms. As shown in Fig. S3 and Fig. 4*A*, the sharp asymmetric in-plane and out-of plane vibrational modes apparent in the ternary complex of hIDO are significantly weaker in hTDO, indicating that the heme group in hTDO is not distorted in the same fashion as that found in hIDO. The splitting of the δ_{vinyl} mode at 421 cm^{-1} into 2 peaks suggests that the 2 vinyl groups of the heme adopt 2 distinct conformations. In the $^{16}O_2$–$^{18}O_2$ isotope difference spectrum, only one $\nu_{Fe\text{-}O2}$ mode at 564 cm^{-1} was observed (see bottom trace in Fig. 4*A*). Similar measurements conducted at 2 s revealed almost identical spectra, confirming the absence of the ferryl intermediate during the hTDO reaction. The data indicate that either the decay of the ferryl species was faster than its formation, such that it did not accumulate to a detectable level, or the hTDO reaction followed an alternate mechanism.

Computational Studies. To delineate the molecular mechanism underlying the experimental observations, we performed computational simulations of the dioxygenase reactions carried out by hIDO and xcTDO (an isoform of TDO from *Xanthomonas campestris*), by using classic molecular dynamics and hybrid QM/MM methods as described in the *SI Text*. The structural and energetic parameters thus obtained are summarized in Table S1. Here, xcTDO was used as a model for hTDO, as the crystallographic structure of the latter is not available; in addition, sequence alignment shows that all of the critical residues involving substrate-protein interactions in xcTDO are well-conserved in hTDO (24).

The calculations show that in both hIDO and xcTDO, the dioxygen gains superoxide character upon binding to the heme iron, as evident by the negative charges on O_2 and the relatively long O-O bond length, consistent with the observed $\nu_{O\text{-}O}$ at 1,137 cm^{-1}. In

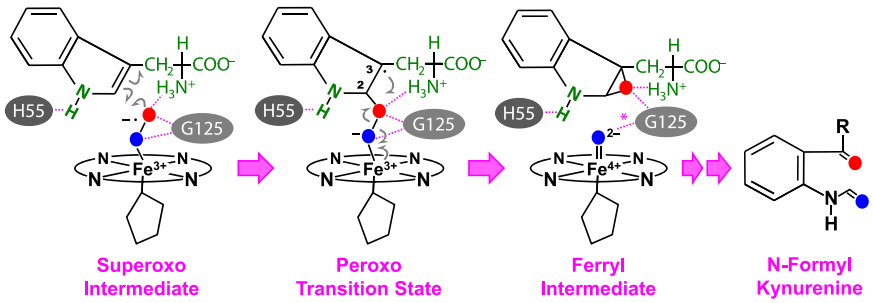

Fig. 5. Proposed ferryl-based dioxygenase mechanism. The scheme is based on the xcTDO reaction; a similar mechanism is applicable to hIDO, except that, in hIDO, the H55 is replaced with S167, which is incapable of accepting an H-bond from the indole amine group of the substrate, the G125 is replaced by A264, and the H-bond (indicated by ''*'') in the ferryl intermediate is absent.

addition, as illustrated in Fig. 5, in both enzymes the ferric heme-bound superoxide in the active ternary complex can be readily inserted into the C_2=C_3 bond of the indole ring, without the deprotonation of the indoleamine, giving rise to the 2-alkylperoxo transition state, in which the C_2 atom assumes a sp^3 configuration, while the C_3 atom retains the sp^2 configuration with a radical associated with it. The 2-alkylperoxo transition state spontaneously converts to an indole 2,3-epoxide and a compound-II type of ferryl intermediate via a homolytic O-O bond cleavage (as evident by the charge distribution listed in Table S1). In the second step of the reaction, the ferryl oxygen presumably can be inserted into the C_2-O or C_2-C_3 bond of the indole 2,3-epoxide intermediate, leading to the NFK product. Additional computational studies are now underway to resolve the associated reaction mechanism.

In the optimized structure of the active ternary complex of xcTDO (Fig. 6*A*), the indole ring of the substrate is held in position by H55 via an H-bond. The 2 atoms of the heme-bound dioxygen accept H-bonds from the amino group of the substrate, as well as the amine group of the G125 residue. The Fe-O-O moiety lies perpendicular to the heme plane and parallel with the indole ring, providing optimum alignment of the O-O bond, with respect to the C_2=C_3 bond, for the insertion of the terminal atom of the dioxygen to the C_2 position of the indole ring, which leads to the 2-alkylperoxo transition state. In the alkylperoxo transition state and the later ferryl intermediate, the H-bonding interactions between the 2 oxygen atoms, L-Trp, H55, and G125 remain intact, indicating that stereoelectronic factors are important for the dioxygenase reaction.

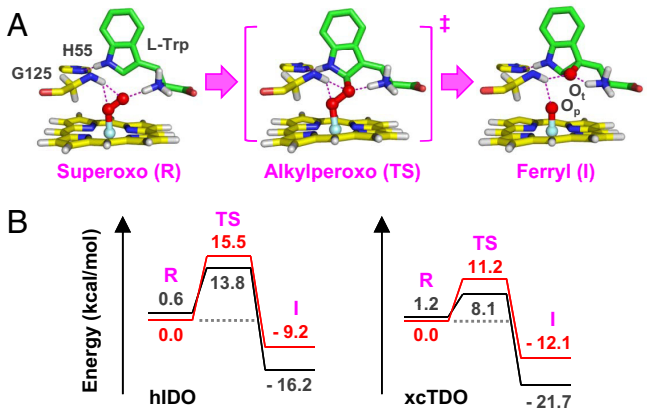

Fig. 6. Optimized structures of the superoxo, peroxo, and ferryl derivatives of xcTDO (*A*) and the associate potential energy diagram with respect to that of hIDO (*B*). The structures were obtained from QM/MM studies. The structural parameters are listed in Table S1. The indole ring of the substrate retains a similar regio-orientation with respect to the heme plane along the reaction coordinate, although in the alkylperoxo transition state it slightly shifts closer to the Fe-O-O moiety and moves back to its original position in the ferryl intermediate. Similar structures were found in hIDO (see Fig. S4*a*), except that in hIDO the indole ring exhibits higher conformational freedom because of the absence of the H-bond between the H55 and the indoleamine group. The potential energy curves in (*B*), colored in red and black, were calculated from the singlet and triplet reactions, respectively (see the *SI Text* and Table S1). I, ferryl intermediate; R, superoxo reactant; TS, alkylperoxo transition state.

In hIDO, H55 is replaced by S167, which abolishes the structural constraint imposed on the indole ring of the substrate. Consequently, the ternary complex of hIDO may assume multiple conformations (Fig. S4*b*). One of the conformers exhibits a conformation similar to that of xcTDO, which we consider as the active species responsible for the turnover of the dioxygenase reaction (Fig. S4*a*). In the superoxo, alkylperoxo, and ferryl species (See Dataset S1, Dataset S2, Dataset S3, Dataset S4, and Dataset S5), the regio-orientation of the Fe-O-O moiety with respect to the substrate, A264 (equivalent to G125 in xcTDO), and the heme are in general similar to those found in xcTDO, with the following exceptions: (*i*) the indole ring of the substrate is more mobile, because of the absence of its H-bonding interaction with H55, and the heme appears to be more flexible and prone to distortion along the reaction coordinate; and (*ii*) in the ferryl intermediate, the H-bond between A264 and the proximal oxygen atom (O_p) is lost because of a slight tilt of the indole ring of the substrate and the associated movement of the A264. These unique structural features of hIDO account for the higher activation energy barrier for the superoxo→ferryl conversion, as well as the destabilization of the ferryl intermediate, as illustrated in Fig. 6*B*. They plausibly also raise the activation barrier for the subsequent oxygen insertion to the indole-2,3-epoxide, accounting for the accumulation of the ferryl intermediate in hIDO, but not in hTDO.

The high conformational freedom of the substrate in hIDO is consistent with its broad $\nu_{Fe\text{-}O2}$ mode (see Fig. 3*C*), as well as its much broader substrate-selectivity as compared to hTDO (3). It is also consistent with its ease of auto-oxidation, as the high degree of conformational freedom presumably increases the solvent accessibility of the distal heme pocket, which has been shown to be an important structural factor leading to auto-oxidation of O_2-derivatives of hemeproteins (50). The dynamic H-bonding network linking the dioxygen and its environment, on the other hand, accounts for the relatively low $\nu_{Fe\text{-}O2}$ frequency and the unusual activation of the typically RR silent $\nu_{O\text{-}O}$ mode (see Fig. 3*A*). Moreover, although the impact of the heme distortion on the catalytic mechanism remains to be further investigated, the flexible nature of the heme in hIDO agrees well with the activation of the asymmetric in-plane and out-of-plane heme modes found in the RR spectrum of hIDO, but not in hTDO (see Fig. S3).

Conclusions

Our data highlight the structural differences between hTDO and hIDO, as well as the importance of stereoelectronic factors in controlling the dioxygenase chemistry carried out by the 2 dioxygenases, which are delicately regulated by the interactions between the ligand, the substrate, and the protein matrix surrounding them. The RR data provide direct evidence for a key ferryl intermediate of hIDO. Combined with molecular dynamics and QM/MM simulations, the data support a model in which the dioxygenase reaction is initiated by the insertion of the

terminal atom of dioxygen into the $C_2=C_3$ bond of the indole ring, giving rise to the ferryl intermediate and an indole 2,3-epoxide, which recombine to generate NFK. They demonstrate that the 2 atoms of the dioxygen in hIDO and hTDO are inserted into the substrate via a consecutive 2-step reaction, in contrast to the widely held hypothesis that the 2 oxygen atoms are simultaneously inserted into the substrate (3).

The sequential oxygen insertion mechanism revealed in this work resembles that of a number of nonheme dioxygenases, such as homoprotocatechuate 2,3-dioxygenase (51), although the details differ significantly between these 2 types of dioxygenases (for the reaction mechanisms of nonheme dioxygenases, see recent reviews in refs. 52 to 55 and references therein). The preference of a sequential mechanism over a concerted mechanism for both the nonheme and heme-based dioxygenases is presumably a result of high energy costs for forming a sterically constrained transition state required for the concerted mechanism. It is noteworthy that a similar sequential dioxygenation mechanism has been implicated by DFT calculations in the reactions carried out by a nonheme dioxygenase, apocarotenoid oxygenase (56) and a heme-Trp model complex (29), although in both cases the sequential mechanism was predicted to be energetically less favorable as compared to the concerted mechanism.

Recently, hIDO research has attracted a great deal of attention, as a result of the recognition of hIDO as a potential therapeutic target for cancer, as well as other diseases in which immunity is impaired (18, 20, 57). Our data does not only help to fill in a major knowledge gap in heme-oxygen chemistry, but they also offer a starting point for additional computational and structural investigations, which are anticipated to provide valuable insights for the development of anticancer drugs specifically targeting hIDO.

Materials and Methods

The stopped-flow measurements were performed by mixing the deoxy enzymes with O_2-containg buffer in a π* 180 system from applied Photophysics Inc. (Leatherhead) as previously reported (28). The continuous-flow RR measurements were performed with instrumentation described elsewhere (32, 40), with the homemade continuous-flow cell modified to accommodate a larger time window. The sample flow rate was 3 ml/min. A 413.1-nm laser line from a Kr^+ laser (Spectra Physics) was used as the excitation source. The experimental details are described in *Materials and Methods* in the *SI Text*.

ACKNOWLEDGMENTS. We thank Drs. Denis L. Rousseau and Jack Peisach for valuable discussions. This work was partially supported by National Institute of Health Molecular Biophysics Training Grant GM008572 (to A.L.-B.) and by the Universidad de Buenos Aires Grant 08-X625 (to M.A.M.), Grant X076 (to D.A.E.), Grant ANPCYT 07–1650 (to M.A.M.), Grant 06–25667 (to D.A.E.), Consejo Nacional de Investigaciones Científicas y Técnicas (CONICET) PIP 5218, and Guggenheim Foundation fellowship (awarded to D.A.E.). D.A.E. and M.A.M. are members of CONICET; L.C. holds a CONICET PhD fellowship. Computer power was provided by the Centro de Computación de Alto Rendimiento at the Facultad de Ciencias Exactas y Naturales-Universidad de Buenos Aires.

1. Groves JT (2004) in *Cytochrome P450: Structure, Mechanism, and Biochemistry*, ed. Ortiz de Montellano PR (Kluwer Academic/Plenum, New York), pp. 1–44.
2. Makris TM, von Koenig K, Schlichting I, Sligar SG (2006) The status of high-valent metal oxo complexes in the P450 cytochromes. *J Inorg Biochem* 100:507–518.
3. Sono M, Roach MP, Coulter ED, Dawson JH (1996) Heme-containing oxygenases. *Chem Rev* 96:2841–2888.
4. Babcock GT, Wikstrom M (1992) Oxygen activation and the conservation of energy in cell respiration. *Nature* 356:301–309.
5. Gennis RB (2004) Coupled proton and electron transfer reactions in cytochrome oxidase. *Front Biosci* 9:581–591.
6. Ogura T, Kitagawa T (2004) Resonance Raman characterization of the P intermediate in the reaction of bovine cytochrome C oxidase. *Biochim Biophys Acta* 1655:290–297.
7. Han S, Takahashi S, Rousseau DL (2000) Time dependence of the catalytic intermediates in cytochrome C oxidase. *J Biol Chem* 275:1910–1919.
8. Dunford HB, Stillman JS (1976) Structure and functional properties of peroxidases and catalases. *Coord Chem Rev* 19:187–251.
9. Poulos TL, Kraut J (1980) The stereochemistry of peroxidase catalysis. *J Biol Chem* 255:8199–8205.
10. Hayaishi O (1976) Properties and function of indoleamine 2,3-dioxygenase. *J Biochem* (*Tokyo*) 79(4):13–21.
11. Feigelson O, Brady FO (1974) in *Molecular Mechanism of Oxygen Activation* (Academic Press, New York), pp. 87–133.
12. Hayaishi O, Takikawa O, Yoshida R (1990) Indoleamine 2,3-dioxygenase: properties and functions of a superoxide utilizing enzyme. *Prog Inorg Chem* 38:75–95.
13. Schutz G, Feigelson P (1972) Purification and properties of rat liver tryptophan oxygenase. *J Biol Chem* 247(17):5327–5332.
14. Greengard O, Feigelson P (1961) The activation and induction of rat liver tryptophan pyrrolase in vivo by its substrate. *J Biol Chem* 236(1):158–161.
15. Schutz G, Killewich L, Chen G, Feigelson P (1975) Control of the mRNA for hepatic tryptophan oxygenase during hormonal and substrate induction. *Proc Natl Acad Sci USA* 72:1017–1020.
16. Schimke RT, Sweeney EW, Berlin CM (1965) The roles of synthesis and degradation in the control of rat liver tryptophan pyrrolase. *J Biol Chem* 240:322–331.
17. Yamamoto S, Hayaishi O (1967) Tryptophan pyrrolase of rabbit intestine. D- and L-tryptophan-cleaving enzyme or enzymes. *J Biol Chem* 242:5260–5266.
18. Muller AJ, Prendergast GC (2007) Indoleamine 2,3-dioxygenase in immune suppression and cancer. *Curr Cancer Drug Targets* 7(1):31–40.
19. Takikawa O (2005) Biochemical and medical aspects of the indoleamine 2,3-dioxygenase-initiated L-tryptophan metabolism. *Biochem Biophys Res Commun* 338(1):12–19.
20. Munn DH, Mellor AL (2007) Indoleamine 2,3-dioxygenase and tumor-induced tolerance. *J Clin Invest* 117:1147–1154.
21. Hamilton GA (1969) Mechanisms of two- and four-electron oxidations catalyzed by some metalloenzymes. *Adv Enzymol Relat Areas Mol Biol* 32:55–96.
22. Leeds JM, Brown PJ, McGeehan GM, Brown FK, Wiseman JS (1993) Isotope effects and alternative substrate reactivities for tryptophan 2,3-dioxygenase. *J Biol Chem* 268:17781–17786.
23. Sugimoto H, et al. (2006) Crystal structure of human indoleamine 2,3-dioxygenase: catalytic mechanism of O2 incorporation by a heme-containing dioxygenase. *Proc Natl Acad Sci USA* 103:2611–2616.
24. Forouhar F, et al. (2007) Molecular insights into substrate recognition and catalysis by tryptophan 2,3-dioxygenase. *Proc Natl Acad Sci USA* 104:473–478.
25. Zhang Y, et al. (2007) Crystal structure and mechanism of tryptophan 2,3-dioxygenase, a heme enzyme involved in tryptophan catabolism and in quinolinate biosynthesis. *Biochemistry* 46(1):145–155.
26. Batabyal D, Yeh SR (2007) Human tryptophan dioxygenase: a comparison to indoleamine 2,3-dioxygenase. *J Am Chem Soc* 129:15690–15701.
27. Terentis AC, et al. (2002) The heme environment of recombinant human indoleamine 2,3-dioxygenase. Structural properties and substrate-ligand interactions. *J Biol Chem* 277:15788–15794.
28. Batabyal D, Yeh SR (2009) Substrate-protein interaction in human tryptophan dioxygenase: the critical role of H76. *J Am Chem Soc* 131:3260–3270.
29. Chung LW, Li X, Sugimoto H, Shiro Y, Morokuma K (2008) Density functional theory study on a missing piece in understanding of heme chemistry: the reaction mechanism for indoleamine 2,3-dioxygenase and tryptophan 2,3-dioxygenase. *J Am Chem Soc* 130:12299–12309.
30. Ishimura Y, Nozaki M, Hayaishi O (1970) The oxygenated form of L-tryptophan 2,3-dioxygenase as reaction intermediate. *J Biol Chem* 245:3593–3602.
31. Sono M, Taniguchi T, Watanabe Y, Hayaishi O (1980) Indoleamine 2,3-dioxygenase. Equilibrium studies of the tryptophan binding to the ferric, ferrous, and CO-bound enzymes. *J Biol Chem* 255:1339–1345.
32. Takahashi S, et al. (1997) Folding of cytochrome C initiated by submillisecond mixing. *Nat Struct Biol* 4(4):44–50.
33. Hu S, Smith KM, Spiro TG (1996) Assignment of protoheme resonance Raman spectrum by heme labeling in myoglobin. *J Am Chem Soc* 118:12638–12646.
34. Li XY, Czernuszewicz RS, Kincaid JR, Stein P, Spiro TG (1990) Consistent porphyrin force field. 2. Nickel octaethylporphyrin skeletal and substituent mode assignments from nitrogen-15, meso-d4, and methylene-d16 Raman and infrared isotope shifts. *J Phys Chem* 94(1):47–61.
35. Hu S, Morris IK, Singh JP, Smith KM, Spiro TG (1993) Complete assignment of cytochrome C resonance Raman spectra via enzymic reconstitution with isotopically labeled hemes. *J Am Chem Soc* 115:12446–12458.
36. Cheung LD, Chang CC, Yu NT, Shelnutt JA (1977) Resonance Raman spectra of metalloporphyrins. Effects of Jahn-Teller instability and nuclear distortion on excitation profiles of Stokes fundamentals. *J Chem Phys* 66:3387–3398.
37. Huang Q, Medforth CJ, Schweitzer-Stenner R (2005) Nonplanar heme deformations and excited state displacements in nickel porphyrins detected by Raman spectroscopy at Soret excitation. *J Phys Chem A* 109:10493–10502.
38. Felton RH, Yu N-T (1978) in *The Porphyrins*, ed. Dolphin D. (Academic, New York), Vol. 3, pp. 347–393.
39. Jarzeücki AA, Spiro TG (2005) Porphyrin distortion from resonance Raman intensities of out-of-plane modes: computation and modeling of N-methylmesoporphyrin, a ferrochelatase transition state analog. *J Phys Chem A* 109:421–430.
40. Lu C, Egawa T, Mukai M, Poole RK, Yeh SR (2008) Hemoglobins from *Mycobacterium tuberculosis* and *Campylobacter jejuni*: a comparative study with resonance Raman spectroscopy. *Methods Enzymol* 437:255–286.
41. Bruha A, Kincaid JR (1988) Resonance Raman studies of dioxygen adducts of cobalt-substituted heme proteins and model compounds. Vibrationally coupled dioxygen and the issues of multiple structures and distal side hydrogen bonding. *J Am Chem Soc* 110:6006–6014.

42. Drago RS, Corden BB (1980) Spin-pairing model of dioxygen binding and its application to various transition-metal systems as well as hemoglobin cooperativity. *Acc Chem Res* 13:353–360.
43. Terner J, et al. (2006) Resonance Raman spectroscopy of oxoiron(IV) porphyrin pi-cation radical and oxoiron(IV) hemes in peroxidase intermediates. *J Inorg Biochem* 100:480–501.
44. Nakamoto K (2002) Resonance Raman spectra and biological significance of high-valent iron(IV,V) porphyrins. *Coord Chem Rev* 226(1-2):153–165.
45. Davies DM, Jones P, Mantle D (1976) The kinetics of formation of horseradish peroxidase compound I by reaction with peroxobenzoic acids. pH and peroxo acid substituent effects. *Biochem J* 157:247–253.
46. Mak PJ, et al. (2007) Resonance Raman detection of the hydroperoxo intermediate in the cytochrome P450 enzymatic cycle. *J Am Chem Soc* 129:6382–6383.
47. Denisov IG, Mak PJ, Makris TM, Sligar SG, Kincaid JR (2008) Resonance Raman characterization of the peroxo and hydroperoxo intermediates in cytochrome P450. *J Phys Chem Acta* 112:13172–13179.
48. Ibrahim M, Denisov IG, Makris TM, Kincaid JR, Sligar SG (2003) Resonance Raman spectroscopic studies of hydroperoxo-myoglobin at cryogenic temperatures. *J Am Chem Soc* 125:13714–13718.
49. Mak PJ, Kincaid JR (2008) Resonance Raman spectroscopic studies of hydroperoxo derivatives of cobalt-substituted myoglobin. *J Inorg Biochem* 102:1952–1957.
50. Brantley RE, Jr, Smerdon SJ, Wilkinson AJ, Singleton EW, Olson JS (1993) The mechanism of autooxidation of myoglobin. *J Biol Chem* 268:6995–7010.
51. Kovaleva EG, Lipscomb JD (2007) Crystal structures of Fe2+ dioxygenase superoxo, alkylperoxo, and bound product intermediates. *Science* 316:453–457.
52. Lipscomb JD (2008) Mechanism of extradiol aromatic ring-cleaving dioxygenases. *Curr Opin Struct Biol* 18:644–649.
53. Bugg TD, Ramaswamy S (2008) Non-heme iron-dependent dioxygenases: unravelling catalytic mechanisms for complex enzymatic oxidations. *Curr Opin Chem Biol* 12:134–140.
54. Koehntop KD, Emerson JP, Que L, Jr (2005) The 2-His-1-carboxylate facial triad: a versatile platform for dioxygen activation by mononuclear non-heme iron(II) enzymes. *J Biol Inorg Chem* 10(2):87–93.
55. Bassan A, Blomberg MR, Siegbahn PE (2004) A theoretical study of the cis-dihydroxylation mechanism in naphthalene 1,2-dioxygenase. *J Biol Inorg Chem* 9:439–452.
56. Borowski T, Blomberg MR, Siegbahn PE (2008) Reaction mechanism of apocarotenoid oxygenase (ACO): a DFT study. *Chemistry* 14:2264–2276.
57. Muller AJ, DuHadaway JB, Donover PS, Sutanto-Ward E, Prendergast GC (2005) Inhibition of indoleamine 2,3-dioxygenase, an immunoregulatory target of the cancer suppression gene Bin1, potentiates cancer chemotherapy. *Nat Med* 11:312–319.